Clim. Past Discuss., 9, 6287–6309, 2013
www.clim-past-discuss.net/9/6287/2013/
doi:10.5194/cpd-9-6287-2013

Climate of the Past
Discussions
Open Access

Variability of the Asian summer monsoon during the penultimate glacial/interglacial period inferred from stalagmite oxygen isotope records from Yangkou cave, Chongqing, Southwestern China

T.-Y. Li[1,2,3], C.-C. Shen[3], L.-J. Huang[3], X.-Y. Jiang[4], X.-L. Yang[1], H.-S. Mii[5], S.-Y. Lee[6], and L. Lo[3]

[1]Key Laboratory of Eco-environments in Three Gorges Reservoir Region, Ministry of Education, School of Geographical Sciences, Southwest University, Chongqing, 400715, China
[2]State Key Laboratory of Loess and Quaternary Geology, Institute of Earth Environment, CAS, Xi'an, 710075, China
[3]High-Precision Mass Spectrometry and Environment Change Laboratory (HISPEC), Department of Geosciences, National Taiwan University, Taipei, 10617, Taiwan
[4]College of Geographical Science, Fujian Normal University, Fuzhou, 350007, China
[5]Department of Earth Sciences, National Taiwan Normal University, Taipei, 11677, Taiwan
[6]Research Center for Environmental Changes, Academia Sinica, Taipei, 11529, Taiwan

Received: 29 October 2013 – Accepted: 31 October 2013 – Published: 11 November 2013

Correspondence to: C.-C. Shen (river@ntu.edu.tw)

Published by Copernicus Publications on behalf of the European Geosciences Union.

Abstract

The orbital-timescale dynamics of the Quaternary Asian summer monsoons (ASM) are frequently attributed to precession-dominated Northern Hemisphere summer insolation. However, this ASM variability is inferred primarily from oxygen isotope records of stalagmites, mainly from Sanbao cave in mainland China, and may not provide a comprehensive picture of ASM evolution. A new spliced stalagmite oxygen isotope record from Yangkou cave tracks summer monsoon precipitation variation from 124–206 thousand years ago in Chongqing, southwest China. When superimposed on the Sanbao record, the Yangkou-inferred precipitation time series is shown to support the strong ASM periods at marine isotope stages (MIS) 6.3, 6.5, and 7.1 and weak ASM intervals at MIS 6.2, 6.4, and 7.0. This consistency confirms that ASM events affected most of mainland China. We show that change in glacial/interglacial (G/IG) ASM intensity was also governed by the Walker Circulation by combining our results with published paleo-Pacific thermal and salinity records. One of the strongest ASM events over the past fiver G/IG cycles, at MIS 6.5, was enhanced by such zonal forcing associated with prevailing trade winds in the Pacific.

1 Introduction

Climate in East Asia, the most densely populated region in the world, is profoundly influenced by the Asian monsoon (AM). Asian summer monsoon (ASM) precipitation strongly governs regional vegetation, agriculture, culture, and economies (e.g. Cheng et al., 2012a), and even affected the stability of Chinese dynastic rule (Zhang et al., 2008; Tan et al., 2011). Recent studies have led to significant advances in understanding Quaternary ASM evolution on different time scales (e.g. An, 2000; Wang et al., 2001, 2008; Fleitmann et al., 2003, 2004; Cheng et al., 2009, 2012b; Zhang et al., 2008; Sinha et al., 2011).

CPD
9, 6287–6309, 2013

Our current understanding of ASM variation over past 500 kyr BP (before 1950 AD) has been reconstructed using oxygen isotope records of Chinese stalagmites (Wang et al., 2008; Cheng et al., 2012b) with the advantages of absolute and high-precision chronologies (e.g. Cheng et al., 2000, 2013; Shen et al., 2002, 2012). Stalagmite-inferred orbital-scale ASM intensity closely follows the change in precession-dominated Northern Hemisphere (NH) summer insolation (NHSI) (Wang et al., 2008; Cheng et al., 2012b). However, these 100s-kyr records were mainly from a single cave, namely Sanbao cave, located in Hubei Province, China (Fig. 1; Wang et al., 2008; Cheng et al., 2012b). Utilizing only one site leads to uncertainties in the spatial extent of Quaternary ASM evolution. These uncertainties stem from differences in local or regional climatic and environmental conditions (Lachniet, 2009), hydrological variability of monsoonal sources (e.g. Dayem et al., 2010; Clemens et al., 2010; Pausata et al., 2011), and interactions between climatic subsystems (e.g. Maher and Thompson, 2012; Tan, 2013).

Sanbao records, for example, show distinct ASM events at marine isotope stages (MIS) 6.3 and 6.5 during the penultimate glacial time and a weaker summer monsoon during the penultimate glacial maximum (PGM) at MIS 6.2 (Fig. 1 of Wang et al., 2008). To clarify whether this combination of weak PGM ASM intensities and strong ASM events during the penultimate glacial/interglacial (G/IG) period are local effects, we built an integrated stalagmite oxygen stable isotope record from Yangkou cave, Chongqing, China, covering 124–206 kyr BP (Fig. 1). Comparison with records from other Chinese caves would confirm the fidelity of Sanbao cave-inferred ASM intensities. Our results also demonstrate that a strong Walker circulation in the Pacific could enhance glacial ASM precipitation.

2 Material and methods

2.1 Regional settings and samples

Stalagmites were collected from Yangkou cave (29°2′ N, 107°11′ E; altitude: 2140 m; length: 2245 m), located at Jinfo Mountain National Park, Chongqing City, southwestern China (Fig. 1) during two field trips in October 2010 and July 2011. The cave, developed in Permian limestone bedrock, is 400 km southwest of Sanbao cave (31°40′ N, 110°26′ E) in Hubei Province (Wang et al., 2008). The cave air temperature is 7.5 °C and the average relative humidity is > 80 % (October 2011–October 2013). The regional climate is dominated by the AM and annual rainfall is 1400–1500 mm, 83 % from April to October (Zhang et al., 1998). Five stalagmites, YK05, YK12, YK23, YK47 and YK61, which formed within a time interval of 120–210 kyr BP were halved and polished for ^{230}Th dating and oxygen stable isotope analysis.

2.2 ^{230}Th dating

Chemistry and instrumental analysis were conducted in the High-Precision Mass Spectrometry and Environment Change Laboratory (HISPEC), Department of Geosciences, National Taiwan University. Fifty three powdered subsamples, 60–80 mg each, were drilled from the polished surface along the deposit lamina of the five stalagmites (Fig. 2, Table 1), on a class-100 bench in a class-10 000 subsampling room. Uranium-thorium (U-Th) chemistry (Shen et al., 2003) was performed in a class-10 000 clean room with independent class-100 benches and hoods (Shen et al., 2008). A multi-collector inductively coupled plasma mass spectrometer (MC-ICP-MS), Thermo Fisher Neptune, with secondary electron multiplier protocols, was used for the determination of U-Th isotopic contents and compositions (Shen et al., 2012). All errors of U-Th isotopic data and ^{230}Th dates are two standard deviations (2σ) unless otherwise noted.

CPD
9, 6287–6309, 2013

2.3 Stable isotopes

Five-to-seven coeval subsamples, 60–120 µg each, were drilled from one layer per stalagmite to measure the oxygen and carbon isotopic compositions as part of the so-called "Hendy Test" (Hendy, 1971). To obtain oxygen time series, 604 subsamples, 60–120 µg each, were drilled at 0.5–3.0 mm intervals along the maximum growth axis. Measurement of oxygen stable isotopes was performed by two isotope ratio mass spectrometers, including a Finnigan Delta V Plus in the Southwest University, China and a Micromass IsoPrime instrument at the National Taiwan Normal University. Oxygen isotope values were reported as $\delta^{18}O$ (‰) with respect to the Vienna Pee Dee Belemnite standard (V-PDB). An international standard, NBS-19, was used in both laboratories to confirm that the 1-sigma standard deviation of $\delta^{18}O$ was better than ±0.1 ‰.

3 Results and discussion

3.1 Chronology

U-Th isotopic and concentration data and ^{230}Th dates of all stalagmite subsamples are given in Table 1. High uranium levels range from 0.8–13 ppm and relatively low thorium contents from 10 000–100 s ppt. Corrections for initial ^{230}Th are less than 90 yr, much smaller than dating uncertainties of 100 s–1800 yr that are common for stalagmites with these ^{230}Th ages (Table 1). Determined age intervals are 179.6–189.8, 133.7–181.9, 172.6–206.8, 130.0–132.1, and 97.2–172.5 kyr BP for stalagmites YK05, YK12, YK23, YK47, and YK61, respectively (Fig. 3). One-to-two hiatuses are observed for stalagmites, YK12, YK23, and YK61 (Figs. 2 and 3). The chronology of each stalagmite was developed using linear interpolation between ^{230}Th dates, which are all in stratigraphic order (Fig. 3).

3.2 Yangkou oxygen isotope data

The well-known Hendy Test has been taken as an essential requirement when assessing the ability of stalagmites to serve as paleoclimate archives (Hendy, 1971) (Fig. 4). Despite relative large δ^{13}C variations of 0.2–0.4 ‰ (1σ) for coeval subsamples on the five selected layers (Fig. 4a), only a small variations in δ^{18}O of ±0.1–0.2 ‰ (1σ) are observed on individual horizons of coeval subsamples (Fig. 4b). Also, there is no relationship between δ^{18}O and δ^{13}C values, which is an additional part of the Hendy Test (Fig. 4c). The replication of the δ^{18}O records both within Yangkou cave (Fig. 5) and between Chinese caves (Fig. 6), as well as successful Hendy Tests, indicates that the stalagmites formed under an oxygen isotopic equilibrium condition. The Yangkou stalagmite δ^{18}O data therefore represent rainfall oxygen isotopic change, which is a reflection of regional hydrological variability in the AM territory (e.g. Wang et al., 2001, 2008; Cheng et al., 2009; Li et al., 2011).

The oxygen isotope sequences for all of the Yangkou stalagmites are illustrated in Fig. 5a. The spliced record covers a time interval from 124–206 kyr BP, with three narrow hiatuses at 132.1–133.5, 190.4–193.2, and 200.3–200.9 kyr BP. This δ^{18}O record varies from −10 ∼ −9 ‰ at 124–127, 141–155, 165–177, and 193–201 kyr BP, to −7 ∼ −6 ‰ at 128–136, 155–165, 177–190, and 201–206 kry BP. The highest δ^{18}O data of −5 ∼ −4 ‰ occurs at 128–136 kyr BP, the PGM.

3.3 Comparison with other Chinese stalagmite records

The new spliced stalagmite δ^{18}O sequence from Yangkou cave over the time period of 124–206 kyr BP shows four strong ASM intervals at MIS 5.5, 6.3, 6.5, and 7.1 and four weak ASM intervals corresponding to MIS 6.2, MIS 6.4, MIS 7.0, and MIS 7.2 (Fig. 5a). This variation of stalagmite-inferred ASM recorded in Yangkou cave is aligned with previous ASM changes from other Chinese caves, such as Sanbao (Wang et al., 2008; Cheng et al., 2009) and Hulu (32°30′ N, 119°1′ E) (Cheng et al., 2006), from MIS 5.5–7.2 (Fig. 5).

Onsets of strong ASM intervals at MIS 5.5, 6.5, and 7.1 are at 128.3 ± 0.8, 179.9 ± 0.9, and 201.5 ± 1.1 kyr BP respectively in the Yangkou record and concurrent with their counterparts in Sanbao (Wang et al., 2008; Cheng et al., 2009) and Hulu (Cheng et al., 2006). Transients from strong to weak ASM states occur at 135–136 kyr BP during MIS 6.2–6.3 and 164–165 kyr BP during MIS 6.4–6.5. These also match changes in the Sanbao and Hulu records.

Over the past 200 kyr BP, the weakest ASM interval has been suggested to be at MIS 6.2 in the Sanbao records (Wang et al., 2008). For example, the δ^{18}O data are 1 ‰ higher than those at weak ASM intervals of MIS 6.4, 7.0, and 7.2 (Fig. 5). Concurrence between ASM records and ice-rafted debris events in the North Atlantic supports the hypothesis of a forcing on the ASM from NH high-latitudes (Cheng et al., 2009). δ^{18}O values at MIS 6.2 in Yangkou record are 1.5–2 ‰ higher than those at MIS 6.4, 7.0, and 7.2 (Fig. 5). This large difference suggests that this event in Chongqing may have been relatively intensified through NH forcing as compared with the Hubei regions during the PGM.

The Sanbao record indicates that the strongest ASM condition over the past 500 kyr BP occurs in MIS 6.5 (Cheng et al., 2012b). This ASM event, lasting 13 kyr, is 3 kyr longer than a comparable event (in terms of intensity) at interglacial MIS 5.3, and was stronger than at any time during MIS 1, 5.5, 7.3, 9.5, and 11.3, which had higher sea-levels and thermal conditions (Fig. 1 of Cheng et al., 2012b). The lowest contemporaneous δ^{18}O data in the Yangkou record (Fig. 5) show a similar ASM intensity at MIS 6.5 in southwest China.

Overall, consistency of the stalagmite δ^{18}O sequences between Yangkou and other Chinese caves supports the idea that ASM intensity primarily follows NHSI on orbital timescales and is driven by precessional forcing and is punctuated by NH high-latitude climatic fluctuations (e.g. Wang et al., 2001, 2008; Cheng et al., 2009). Agreement in the amplitude and the transition of δ^{18}O dynamics during different MIS also confirms that the Sanbao stalagmite-inferred ASM events, including a very weak one at MIS 6.2

CPD
9, 6287–6309, 2013

and the strongest one at MIS 6.5, are predominant over the entire mainland during the past five G/IG cycles (Cheng et al., 2012b) (Fig. 6).

3.4 Forcings for the abnormal strong ASM at MIS 6.5

The extraordinarily strong ASM condition at MIS 6.5 during the penultimate glacial period is one of the most striking features revealed by new Chinese cave records (Fig. 5). Wang et al. (2008) found a correlation between the stalagmite-inferred ASM intensity and the atmospheric $\delta^{18}O$ records from Antarctic Vostok ice core O_2 bubbles (Sowers et al., 1991; Petit et al., 1999), and suggested that the Dole effect (Dole, 1936; Bender et al., 1994) can explain this similarity. A low atmospheric $\delta^{18}O$ ($\delta^{18}O_{atm}$) peak at 170 kyr BP in the Vostok ice core (Petit et al., 1999), for example, matches the strong-ASM period at MIS 6.5.

The Dole effect was first described by Dole in 1936. This effect is an inequality of $\delta^{18}O$ values between the atmosphere and seawater. Modern $\delta^{18}O$ of atmospheric O_2 ($\delta^{18}O_{atm}$) is ~ 23.5 ‰ heavier than the seawater value (Kroopnick and Craig, 1972). This inequality is caused by respiration, which prefers depleted $^{16}O_2$ rather than $^{18}O_2$, and is balanced by photosynthesis, which emits oxygen with the $\delta^{18}O$ value equal to the water used in the reaction (Guy et al., 1989), resulting in a net decrease of the $\delta^{18}O_{atm}$ value. Accordingly, the $\delta^{18}O_{atm}$ variation can depend on the activity of photosynthesis. Vostok ice core-inferred $\delta^{18}O_{atm}$ evolution most likely results from changes of summer insolation and precipitation in NH, where land provides space for the growth of vegetation and intense photosynthesis during glacial periods (Sun et al., 2000). The summer insolation at MIS 6.5 is less than the interglacial periods at MIS 5.5 and 7.3 (Fig. 5), suggesting that the strong ASM intensity should be associated with additional forcing(s).

Climate conditions around Yangkou and Sanbao caves are influenced by the Indian summer monsoon (ISM) and East Asian summer monsoon (EASM) (Fig. 1). The ISM, a typical tropical monsoon system, is driven by a south-north land-sea thermal gradient;

CPD
9, 6287–6309, 2013

instead, the EASM is controlled by both south-north and east-west land-sea gradients (Wang and Lin, 2002). The EASM precipitation is influenced by the Northwestern Pacific Tropical High, developed by the mainland-Pacific thermal gradient (Wang et al., 2003). The Pacific climatic variability can, therefore, affect EASM precipitation (Tan, 2013).

Cai et al. (2010) and Jiang et al. (2011) argued for a significant impact of the western tropical Pacific sea surface temperature (SST) on the EASM precipitation. They proposed that the evolution and spatial asynchroneity of stalagmite-inferred Holocene precipitation histories at different AM regions could be attributed to SST changes in the western Pacific. Planktonic foraminiferal-inferred SST records of the marine sediment core ODP806B (0°19′ N, 159°22′ E) in the western Pacific warm pool (WPWP) and TR163-19 (2°16′ N, 90°57′ W) in the eastern equatorial Pacific (EEP) (Lea et al., 2000) are plotted in Fig. 6, along with the LR04 stacked benthic δ^{18}O sequence (Lisiecki and Raymo, 2005) and Yangkou and Sanbao cave time series. A SST gradient between the WPWP and EEP during the glacial periods of MIS 6 and 8 is 2 °C, larger than 0.5–1.5 °C gradient during the warm interglacial windows of MIS 5.5 and 7 (Fig. 6). Combined with salinity gradient data, Lea et al. (2000) suggested that the transport of water vapor to the western Pacific was enhanced during glacial times. This large SST gradient could result in an enhanced Walker circulation in the Pacific, similar to the modern La Niña state, which moves the rainfall zone westward and intensifies EASM precipitation (Clement et al., 1999) (Fig. 1). Under a weak Walker circulation, analogous to present El Niño conditions, the rainfall zone in the Pacific migrated eastward and EASM precipitation was reduced (Clement et al., 1999). The extremely strong EASM precipitation at MIS 6.5 was not only governed by high NHSI, but also enhanced by the Pacific SST gradient.

Our arguments are also supported by modern meteorological observations (e.g. Xue et al., 2007; Tan, 2013) and decadally-resolved marine records (Oppo et al., 2009). La Niña years accompany above-normal precipitation probabilities above normal in mainland China (Tan, 2013 and references therein). Two thousand year-SST and

-salinity records from the Makassar Strait (Oppo et al., 2009) also support a strong link between Pacific Ocean climate and the AM.

4 Conclusions

In this study, our new spliced δ^{18}O record of five stalagmites from Yangkou cave, Chongqing, exhibits ASM variability over the time period during 124–206 kyr BP. The prominent consistency between the Yangkou and previous Chinese cave δ^{18}O sequences confirms the duration and intensity of the enclosed ASM events in the entire mainland. Our data supports the hypothesis that the ASM change primarily follows NHSI on a precessional orbital timescale. The weakest ASM condition during low-insolation MIS 6.2 was influenced by meridional forcing originating from the North Atlantic. The strongest ASM intensity in the past 500 kyr BP, at MIS 6.5 (Cheng et al., 2012b), was partially due to zonal forcing associated with G/IG dynamics of Walker circulation in the Pacific.

Acknowledgements. We thank J. W. Partin of the Institute for Geophysics, University of Texas-Austin, and G. S. Burr of the Department of Physics, University of Arizona, for their constructive comments. This work was supported by the Taiwan ROC National Science Council and National Taiwan University grants (101-2116-M-002-009, 102-2116-M-002-016 and 101R7625 to CCS). This study was also supported by grants under the National Natural Science Foundation of China (NSFC) (41030103 and 41172165 to TYL, 41072141 and 41272192 to XLY), the Fundamental Research Funds for the Central Universities (XDJK2013A012 to TYL), and the Opening fund of the State Key Laboratory of Loess and Quaternary Geology (SKLLQG1310 to TYL).

References

An, Z.: The history and variability of the East Asian paleomonsoon climate, Quaternary Sci. Rev., 19, 171–187, 2000.

Bender, M., Sowers, T., and Labeyrie, L.: The Dole Effect and its variations during the last 130 000 years as measured in the Vostok ice core, Global Biogeochem. Cy., 8, 363–376, 1994.

Cai, Y. J., Tan, L., Cheng, H., An, Z., Edwards, R. L., Kelly, M. J., Kong, X., and Wang, X.: The variation of summer monsoon precipitation in Central China since the last deglaciation, Earth Planet. Sc. Lett., 291, 21–31, 2010.

Cheng, H., Edwards, R. L., Hoff, J., Gallup, C. D., Richards, D. A., and Asmersom, Y.: The half-lives of uranium-234 and thorium-230, Chem. Geol., 169, 17–33, 2000.

Cheng, H., Edwards, R. L., Wang, Y., Kong, X., Ming, Y., Kelly, M. J., Wang, X., Gallup, C. D., and Liu, W.: A penultimate glacial monsoon record from Hulu Cave and two-phase glacial terminations, Geology, 34, 217–220, 2006.

Cheng, H., Edwards, R. L., Broecker, W. S., Denton, G. H., Kong, X., Wang, Y., Zhang, R., and Wang, X.: Ice age terminations, Science, 326, 248–252, 2009.

Cheng, H., Sinha, A., Wang, X., Cruz, F. W., and Edwards, R. L.: The global paleomonsoon as seen through speleothem records from Asia to the Americas, Clim. Dynam., 39, 1045–1062, 2012a.

Cheng, H., Zhang, P., Spötl, C., Edwards, R. L., Cai, Y., Zhang, D., Sang, W., Tan, M., and An, Z.: The climatic cyclicity in semiarid-arid Central Asia over the past 500 000 years, Geophys. Res. Lett., 39, L01705, doi:10.1029/2011GL050202, 2012b.

Cheng, H., Edwards, R. L., Shen, C.-C., Polyak, V. J., Asmerom, Y., Woodhead, J., Hellstrom, J., Wang, Y., Kong, X., and Spötl, C.: Improvements in ^{230}Th dating, ^{230}Th and ^{234}U half-life values, and U-Th isotopic measurements by multi-collector inductively coupled plasma mass spectroscopy, Earth Planet. Sc. Lett., 371–372, 82–91, 2013.

Clemens, S. C., Prell, W. L., and Sun, Y.: Orbital-scale timing and mechanisms driving Late Pleistocene Indo-Asian summer monsoons: reinterpreting cave speleothem δ^{18}O, Paleoceanography, 25, PA4207, doi:10.1029/2010PA001926, 2010.

Clement, A. C., Seager, R., and Cane, M. A.: Orbital controls on the El Niño/Southern Oscillation and the tropical climate, Paleoceanography, 14, 441–456, 1999.

Dayem, K. E., Molnar, P., Battisti, D. S., and Roe, G. H.: Lessons learned from oxygen isotopes in modern precipitation applied to interpretation of speleothem records of paleoclimate from eastern Asia, Earth Planet. Sc. Lett., 295, 219–230, 2010.

Dole, M.: The relative atomic weight of oxygen in water and in air a discussion of the atmospheric distribution of the ixygen isotopes and of the chemical standard of atomic weights, J. Chem. Phys., 4, 268–275, 1936.

Fleitmann, D., Burns, S. J., Neff, U., Mangini, A., and Matter, A.: Changing moisture sources over the last 330 000 years in Northern Oman from fluid-inclusion evidence in speleothems, Quaternary Res., 60, 223–232, 2003.

Fleitmann, D., Burns, S. J., Neff, U., Mudelsee, M., Mangini, A., and Matter, A.: Palaeoclimatic interpretation of high-resolution oxygen isotope profiles derived from annually laminated speleothems from Southern Oman, Quaternary Sci. Rev., 23, 935–945, 2004.

Guy, R. D., Berry, J. A., Fogel, M. L., and Hoering, T. C.: Differential fractionation of oxygen isotopes by cyanide-resistant and cyanide-sensitive respiration in plants, Planta, 177, 483–491, 1989.

Hendy, C. H.: The isotopic geochemistry of speleothems, Part 1, the calculation of the effects of different modes of formation on the isotopic composition of speleothems and their applicability as palaeoclimatic indicators, Geochim. Cosmochim. Acta, 35, 801–824, 1971.

Jiang, X., He, Y., Shen, C.-C., Kong, X., Guo, Y., Li, Z., and Chang, Y.-W.: Stalagmite-inferred Holocene precipitation in northern Guizhou Province, China, and asynchronous termination of the climatic optimum in the Asian monsoon territory, Chinese Sci. Bull., 57, 73–79, 2012.

Kroopnick, P. and Craig, H.: Atmospheric oxygen: isotopic composition and solubility fractionation, Science, 175, 54–55, 1972.

Lachniet, M. S.: Climatic and environmental controls on speleothem oxygen-isotope values, Quaternary Sci. Rev., 28, 412–432, 2009.

Lea, D. W., Pak, D. K., and Spero, H. J.: Climate impact of Late Quaternary Equatorial Pacific sea surface temperature variations, Science, 289, 1719–1724, 2000.

Li, T.-Y., Shen, C.-C., Li, H.-C., Li, J.-Y., Chiang, H.-W., Song, S.-R., Yuan, D.-X., Lin, C. D.-J., Gao, P., Zhou, L. P., Wang, J.-L., Ye, M.-Y., Tang, L.-L., and Xie, S.-Y.: Oxygen and carbon isotopic systematics of aragonite speleothems and water in Furong Cave, Chongqing, China, Geochim. Cosmochim. Acta, 75, 4140–4156, 2011.

Lisiecki, L. E. and Raymo, M. E.: A. Pliocene–Pleistocene stack of 57 globally distributed benthic δ^{18}O records, Paleoceanography, 20, PA1003, doi:10.1029/2004PA001071, 2005.

Maher, B. A. and Thompson, R.: Oxygen isotopes from Chinese caves: records not of monsoon rainfall but of circulation regime, J. Quaternary Sci., 27, 615–624, 2012.
Oppo, D. W., Rosenthal, Y., and Linsley, B. K.: 2000-year-long temperature and hydrology reconstructions from the Indo-Pacific warm pool, Nature, 460, 1113–1116, 2009.
Pausata, F. S. R., Battisti, D. S., Nisancioglu, K. H., and Bitz, C. M.: Chinese stalagmite $\delta^{18}O$ controlled by changes in the Indian monsoon during a simulated Heinrich event, Nat. Geosci., 4, 474–480, 2011.
Petit, J. R., Jouzel, J., Raynaud, D., Barkov, N. I., Barnola, J.-M., Basile, I., Bender, M., Chappellaz, J., Davis, M., Delaygue, G., Delmotte, M., Kotlyakov, V. M., Legrand, M., Lipenkov, V. Y., Lorius, G., Pépin, L., Ritz, C., Saltzman, E., and Stievenard, M.: Climate and atmospheric history of the past 420 000 years from the Vostok ice core, Antarctica, Nature, 399, 429–436, 1999.
Shen, C.-C., Edwards, R. L., Cheng, H., Dorale, J. A., Thomas, R. B., Moran, S. B., Weinstein, S. E., and Hirschmann, M.: Uranium and thorium isotopic and concentration measurements by magnetic sector inductively coupled plasma mass spectrometry, Chem. Geol., 185, 165–178, 2002.
Shen, C.-C., Cheng, H., Edwards, R. L., Moran, S. B., Edmonds, H. N., Hoff, J. A., and Thomas, R. B.: Measurement of attogram quantities of ^{231}Pa in dissolved and particulate fractions of seawater by isotope dilution thermal ionization mass spectroscopy, Anal. Chem., 75, 1075–1079, 2003.
Shen, C.-C., Li, K.-S., Sieh, K., Natawidjaja, D., Cheng, H., Wang, X., Edwards, R. L., Lam, D. D., Hsieh, Y.-T., Fan, T.-Y., Meltzner, A. J., Taylor, F. W., Quinn, T. M., Chiang, H.-W., and Kilbourne, K. H.: Variation of initial $^{230}Th/^{232}Th$ and limits of high precision U-Th dating of shallow-water corals, Geochim. Cosmochim. Acta, 72, 4201–4223, 2008.
Shen, C.-C., Wu, C.-C., Cheng, H., Edwards, R. L., Hsieh, Y.-T., Gallet, S., Chang, C.-C., Li, T.-Y., Lam, D.-D., Kano, A., Hori, M., and Spötl, C.: U-Th isotopic determinations in femtogram quantities and high-precision and high-resolution carbonate ^{230}Th dating by MC-ICP-MS with SEM protocols, Geochim. Cosmochim. Acta, 99, 71–86, 2012.
Sinha, A., Stott, L. D., Berkelhammer, M., Cheng, H., Edwards, R. L., Aldenderfer, M., Mudelsee, M., and Buckley, B.: A global context for megadroughts in monsoon Asia during the past millennium, Quaternary Sci. Rev., 30, 47–62, 2011.

Sowers, T., Bender, M., Raynaud, D., Korotkevich, Y. S., and Orchardo, J.: The δ^{18}O of atmospheric O_2 from air inclusions in the Vostok ice core: timing of CO_2 and ice volume changes during the penultimate deglaciation, Paleoceanography, 6, 679–696, 1991.

Sun, X., Li, X., Luo, Y., and Chen, X.: The vegetation and climate at the last glaciation on the emerged continental shelf of the South China Sea, Palaeogeogr. Palaeocl., 160, 301–316, 2000.

Tan, L., Cai, Y., An, Z., Edwards, R. L., Cheng, H., Shen, C.-C., and Zhang, H.: Centennial- to decadal-scale monsoon precipitation variability in the semi-humid region, Northern China during the last 1860 years: records from stalagmites in Huangye Cave, Holocene, 21, 287–296, 2011.

Tan, M.: Circulation effect: response of precipitation δ^{18}O to the ENSO cycle in monsoon regions of China, Clim. Dynam., doi:10.1007/s00382-013-1732-x, in press, 2013.

Wang, B. and Lin, H.: Rainy season of the Asian-Pacific summer monsoon, J. Climate, 15, 386–396, 2002.

Wang, B., Clemens, S. C., and Liu, P.: Contrasting the Indian and East Asian monsoons: implications on geologic timescales, Mar. Geol., 201, 5–21, 2003.

Wang, Y., Cheng, H., Edwards, R. L., An, Z., Wu, J., Shen, C.-C., and Dorale, J. A.: A high-resolution absolute-dated Late Pleistocene monsoon record from Hulu Cave, China, Science, 294, 2345–2348, 2001.

Wang, Y., Cheng, H., Edwards, R. L., Kong, X., Shao, X., Chen, S., Wu, J., Jiang, X., Wang, X., and An, Z.: Millennial- and orbital-scale changes in the East Asian monsoon over the past 224 000 years, Nature, 451, 1090–1093, 2008.

Xue, J., Zhong, W., and Zhao, Y.: Variations of $\delta^{18}O$ in precipitation in the Zhujiang (Pearl) river delta and its relationship with ENSO event, Sci. Geogr. Sin., 27, 825–830, 2007.

Zhang, P., Cheng, H., Edwards, R. L., Chen, F., Wang, Y., Yang, X., Liu, J., Tan, M., Wang, X., Liu, J., An, C., Dai, Z., Zhou, J., Zhang, D., Jia, J., Jin, L., and Johnson, K. R.: A test of climate, sun, and culture relationships from an 1810 year Chinese cave record, Science, 322, 940–942, 2008.

Zhang, R., Zhu, X., Han, D., Zhang, Y., and Fang, F.: Preliminary study on karst caves of MT. Jinfo, Nanchuan, Chongqing, Carsologica Sin., 17, 196–211, 1998.

CPD
9, 6287–6309, 2013

Variability of the Asian summer monsoon

T. -Y. Li et al.

Title Page
Abstract | Introduction
Conclusions | References
Tables | Figures
Back | Close
Full Screen / Esc
Printer-friendly Version
Interactive Discussion

Table 1. U-Th isotopic compositions and ^{230}Th ages for subsamples of five Yangkou stalagmites on MC-ICP-MS at the HISPEC, NTU.

Subsample ID	Depth (mm)	^{238}U (ppb)	^{232}Th (ppt)	δ^{234}U measured[a]	[^{230}Th/^{238}U] activity[c]	[^{230}Th/^{232}Th] (ppm)[d]	Age (yr) uncorrected	Age (yr BP) corrected[c,e]	δ^{234}U$_{initial}$ corrected[b]
Stalagmite: YK5									
YK5-01	3.0	8730 ± 13	553.0 ± 7.1	215.8 ± 2.1	1.0192 ± 0.0024	265 626 ± 3445	179.706 ± 1325	179.643 ± 1325	358.5 ± 3.7
YK5-02	24.0	7335 ± 14	263.1 ± 7.1	218.4 ± 2.7	1.0235 ± 0.0027	471 128 ± 12563	180.437 ± 1600	180.375 ± 1600	363.6 ± 4.8
YK5-03	57.0	4322.4 ± 7.6	5997 ± 17	192.9 ± 2.3	1.0002 ± 0.0024	11 903 ± 39	181.192 ± 1438	181.102 ± 1438	321.9 ± 4.1
YK5-04	79.0	5041 ± 10	500.2 ± 5.7	187.7 ± 2.9	0.9997 ± 0.0026	166 348 ± 1928	183.234 ± 1713	183.171 ± 1713	315.1 ± 5.0
YK5-05	88.0	5729.6 ± 9.4	356.1 ± 5.1	184.6 ± 2.4	0.9986 ± 0.0027	265 267 ± 3814	184.166 ± 1611	184.103 ± 1611	310.6 ± 4.2
YK5-06	103.0	5375.3 ± 9.9	593.2 ± 5.0	202.1 ± 2.6	1.0161 ± 0.0022	152 028 ± 1290	184.207 ± 1499	184.143 ± 1499	340.1 ± 4.7
YK5-07	128.0	4986.2 ± 8.8	137.6 ± 5.8	201.6 ± 2.3	1.0175 ± 0.0023	608 876 ± 25827	185.061 ± 1436	184.999 ± 1436	340.0 ± 4.1
YK5-08	149.0	6076 ± 14	269.0 ± 5.2	205.0 ± 3.0	1.0259 ± 0.0028	382 638.7082 ± 7471	187.222 ± 1841	187.159 ± 1841	348.1 ± 5.3
YK5-09	177.0	8808 ± 11	1103.7 ± 7.2	215.0 ± 1.9	1.0374 ± 0.0016	136 699 ± 889	187.890 ± 1128	187.826 ± 1128	365.7 ± 3.5
YK5-10	188.0	12 100 ± 19	168.3 ± 6.1	210.0 ± 2.5	1.0368 ± 0.0027	1 230 671 ± 44610	189.876 ± 1694	189.815 ± 1694	359.2 ± 4.7
Stalagmite: YK12									
YK12-01	3.6	6262.6 ± 4.1	3895 ± 24	309.6 ± 1.2	0.9620 ± 0.0015	25 540 ± 164	133.762 ± 462	133.690 ± 462	451.8 ± 1.9
YK12-02	10.5	5016.7 ± 2.5	12 393 ± 25	296.1 ± 1.2	0.9590 ± 0.0017	6410 ± 17	135.884 ± 510	135.777 ± 511	434.7 ± 1.8
YK12-03	21.5	6384.1 ± 3.6	1050 ± 21	296.2 ± 1.1	0.9796 ± 0.0014	98 334 ± 1947	141.426 ± 463	141.362 ± 463	441.8 ± 1.7
YK12-04	40.0	5675.3 ± 5.8	9675 ± 32	273.0 ± 1.6	0.9792 ± 0.0017	9483 ± 34	147.071 ± 670	146.978 ± 670	413.7 ± 2.6
YK12-05	57.5	13 314 ± 13	1488 ± 21	259.4 ± 1.5	0.9840 ± 0.0015	145 382 ± 2094	152.201 ± 622	152.138 ± 622	398.9 ± 2.4
YK12-06	78.0	11 746.6 ± 5.5	1425 ± 24	253.54 ± 0.90	0.9852 ± 0.0013	134 061 ± 2272	154.298 ± 485	154.235 ± 485	392.1 ± 1.5
YK12-07	80.0	8830.3 ± 5.3	38 573 ± 98	212.8 ± 1.2	0.9796 ± 0.0027	3702 ± 14	165.267 ± 1071	165.120 ± 1071	339.4 ± 2.2
YK12-08	92.0	7106.6 ± 3.6	7546 ± 25	199.70 ± 0.89	0.9823 ± 0.0014	15 274 ± 55	171.076 ± 643	170.993 ± 643	323.9 ± 1.5
YK12-09	101.0	9513.1 ± 6.5	4483 ± 23	203.4 ± 1.1	0.9976 ± 0.0013	34 954 ± 182	175.795 ± 717	175.725 ± 717	334.3 ± 2.0
YK12-10	105.0	5118.6 ± 6.7	2378 ± 21	185.4 ± 1.9	0.9924 ± 0.0018	35 265 ± 317	181.021 ± 1132	180.949 ± 1132	309.3 ± 3.3
YK12-11	109.5	6109.1 ± 3.8	572 ± 18	178.4 ± 1.2	0.9875 ± 0.0013	174 125 ± 5633	181.929 ± 770	181.866 ± 770	298.4 ± 2.1
Stalagmite: YK23									
YK23-01	2.4	2893.2 ± 2.3	13 899 ± 26	102.8 ± 1.5	0.8935 ± 0.0018	3070.9 ± 8.0	172.790 ± 1035	172.620 ± 1035	167.6 ± 2.4
YK23-02	9.6	2608.9 ± 1.7	13 210 ± 23	99.6 ± 1.1	0.9008 ± 0.0016	2937.3 ± 7.1	177.700 ± 946	177.525 ± 947	164.5 ± 1.9
	Hiatus								
YK23-03	11.2	2705.2 ± 1.3	1370 ± 17	59.55 ± 0.91	0.8799 ± 0.0016	28 683 ± 355	187.327 ± 1030	187.254 ± 1030	101.1 ± 1.6
YK23-04	14.8	2541.1 ± 1.2	10 313 ± 20	60.06 ± 0.89	0.8830 ± 0.0015	3592.3 ± 8.9	188.729 ± 982	188.571 ± 982	102.4 ± 1.5
	Hiatus								
YK23-05	16.8	3255.5 ± 2.0	1365 ± 14	32.5 ± 1.1	0.8632 ± 0.0012	33 986 ± 363	193.472 ± 994	193.401 ± 994	56.1 ± 1.8
YK23-06	27.6	3084.7 ± 1.5	2354 ± 14	32.53 ± 0.92	0.8671 ± 0.0012	18 764 ± 112	195.871 ± 932	195.791 ± 932	56.6 ± 1.6
YK23-07	35.6	2208.7 ± 1.3	2343 ± 15	47.1 ± 1.0	0.8848 ± 0.0014	13 768 ± 89	197.538 ± 1069	197.451 ± 1069	82.2 ± 1.8
YK23-08	42.4	1917.04 ± 0.90	4503 ± 17	39.3 ± 1.1	0.8795 ± 0.0013	6182 ± 25	199.294 ± 1103	199.175 ± 1103	68.9 ± 1.9
	Hiatus								

CPD
9, 6287–6309, 2013

Table 1. Continued.

Subsample ID	Depth (mm)	^{238}U (ppb)	^{232}Th (ppt)	$\delta^{234}U$ measured[a]	$[^{230}Th/^{238}U]$ activity[c]	$[^{230}Th/^{232}Th]$ (ppm)[d]	Age (yr) uncorrected	Age (yr BP) corrected[c,e]	$\delta^{234}U_{initial}$ corrected[b]
YK23-09	43.0	2720.4 ± 1.5	1128 ± 14	21.23 ± 0.90	0.8633 ± 0.0013	34 369 ± 430	200.953 ± 1095	200.882 ± 1095	37.5 ± 1.7
YK23-10	62.4	3355.3 ± 2.2	698 ± 23	16.2 ± 1.0	0.8657 ± 0.0014	68 753 ± 2263	206.207 ± 1217	206.141 ± 1217	29.0 ± 1.8
YK23-11	77.2	2262.6 ± 1.5	899 ± 19	15.0 ± 1.1	0.8655 ± 0.0015	35 976 ± 777	206.922 ± 1340	206.839 ± 1340	26.9 ± 2.1
Stalagmite: YK47									
YK47-01	118.8	812.37 ± 0.81	6437 ± 11	395.2 ± 1.8	1.0173 ± 0.0022	2120.0 ± 6.0	130.186 ± 610	129.991 ± 612	570.7 ± 2.8
YK47-02	137.5	765.96 ± 0.70	2997.5 ± 7.6	398.9 ± 1.8	1.0295 ± 0.0019	4343 ± 13	132.271 ± 565	132.144 ± 566	579.7 ± 2.8
Stalagmite: YK61									
YK61-01	13.6	3427.4 ± 2.1	13 736 ± 25	295.8 ± 1.2	0.9172 ± 0.0019	3779 ± 10	125.391 ± 512	125.255 ± 513	421.5 ± 1.8
YK61-02	15.5	3636.8 ± 1.9	4502 ± 12	275.4 ± 1.2	0.9027 ± 0.0013	12 039 ± 37	125.800 ± 410	125.715 ± 411	393.0 ± 1.8
YK61-03	17.0	3974.8 ± 2.4	4663 ± 10	261.5 ± 1.2	0.8936 ± 0.0013	12 577 ± 32	126.291 ± 408	126.207 ± 408	373.6 ± 1.8
YK61-04	20.0	3418.6 ± 3.7	1271.0 ± 8.9	302.6 ± 1.8	0.9278 ± 0.0013	41 205 ± 291	126.643 ± 476	126.575 ± 476	432.9 ± 2.6
YK61-05	22.4	1520.4 ± 2.4	3627 ± 33	340.2 ± 2.4	0.9619 ± 0.0024	6658 ± 63	127.602 ± 716	127.496 ± 716	487.8 ± 3.5
YK61-06	26.0	2414.5 ± 4.3	2217 ± 29	315.2 ± 2.4	0.9448 ± 0.0027	16 993 ± 229	128.330 ± 800	128.250 ± 800	453.0 ± 3.6
YK61-07	28.3	4454.4 ± 4.8	801.0 ± 8.8	313.7 ± 1.7	0.9452 ± 0.0013	86 784 ± 959	128.698 ± 470	128.633 ± 470	451.4 ± 2.5
YK61-08	30.1	2434.4 ± 2.3	657.4 ± 8.6	314.5 ± 1.6	0.9479 ± 0.0012	57 958 ± 756	129.213 ± 431	129.146 ± 431	453.1 ± 2.3
YK61-09	40.8	3633.5 ± 4.6	207 ± 25	302.5 ± 2.1	0.9389 ± 0.0019	271 567 ± 32442	129.373 ± 635	129.309 ± 635	436.1 ± 3.2
YK61-10	47.8	3140.5 ± 3.0	132.3 ± 7.0	305.6 ± 1.6	0.9459 ± 0.0013	370 865 ± 19563	130.518 ± 452	130.455 ± 452	441.9 ± 2.3
YK61-11	61.3	5420.5 ± 6.6	3648 ± 10	306.2 ± 1.8	0.9502 ± 0.0016	23 311 ± 67	131.466 ± 546	131.393 ± 546	443.9 ± 2.7
	Hiatus								
YK61-12	63.1	2307.3 ± 1.8	1947.5 ± 8.3	303.9 ± 1.3	0.9801 ± 0.0012	19 171 ± 84	139.776 ± 445	139.699 ± 445	451.0 ± 2.0
YK61-13	74.0	5853.2 ± 7.4	3435 ± 11	287.2 ± 1.7	0.9743 ± 0.0017	27 409 ± 90	142.087 ± 626	142.014 ± 626	429.2 ± 2.7
YK61-14	88.0	3614.8 ± 7.1	352 ± 20	321.2 ± 2.9	1.0365 ± 0.0027	175 586 ± 9727	151.405 ± 1087	151.340 ± 1087	492.7 ± 4.7
YK61-15	110.0	4705.3 ± 8.5	672 ± 16	320.3 ± 2.6	1.0476 ± 0.0026	121 199 ± 2976	154.945 ± 1061	154.880 ± 1061	496.2 ± 4.4
YK61-16	130.0	5173.2 ± 8.0	646 ± 18	303.7 ± 2.3	1.0495 ± 0.0022	138 661 ± 3763	160.250 ± 982	160.184 ± 982	477.6 ± 3.8
YK61-17	137.8	6174.8 ± 8.5	405.3 ± 7.9	299.4 ± 2.0	1.0514 ± 0.0019	264 459 ± 5140	162.165 ± 869	162.102 ± 869	473.5 ± 3.4
YK61-18	167.8	4766.3 ± 5.3	347.8 ± 7.3	274.1 ± 1.7	1.0478 ± 0.0014	237 115 ± 4998	169.056 ± 774	168.993 ± 774	441.9 ± 3.0
YK61-19	185.8	2984.1 ± 2.9	1897.4 ± 9.4	239.0 ± 1.7	1.0238 ± 0.0015	26 585 ± 135	172.561 ± 837	172.487 ± 837	389.2 ± 2.9

Chemistry was performed during 2011–2012 (Shen et al., 2003) and instrumental analyses on MC-ICP-MS (Shen et al., 2012).
Analytical errors are 2σ of the mean.
[a] $\delta^{234}U = ([^{234}U/^{238}U]_{activity} - 1) \times 1000$.
[b] $\delta^{234}U_{initial}$ corrected was calculated based on ^{230}Th age (T), i.e. $\delta^{234}U_{initial} = \delta^{234}U \times e^{\lambda_{234} \cdot T}$, and T is corrected age.
[c] $[^{230}Th/^{238}U]_{activity} = 1 - e^{-\lambda_{230}T} + (\delta^{234}U/1000)[\lambda_{230}/(\lambda_{230} - \lambda_{234})](1 - e^{-(\lambda_{230}-\lambda_{234})T})$, where T is the age.
Decay constants used are available in Cheng et al. (2000).
[d] The degree of detrital ^{230}Th contamination is indicated by the $[^{230}Th/^{232}Th]$ atomic ratio instead of the activity ratio.
[e] Age [yr BP (before 1950 AD)] corrections were made using an $^{230}Th/^{232}Th$ atomic ratio of 4 ± 2 ppm.
Those are the values for material at secular equilibrium, with the crustal $^{232}Th/^{238}U$ value of 3.8. The errors are arbitrarily assumed to be 50 %.

CPD
9, 6287–6309, 2013

Variability of the Asian summer monsoon

T. -Y. Li et al.

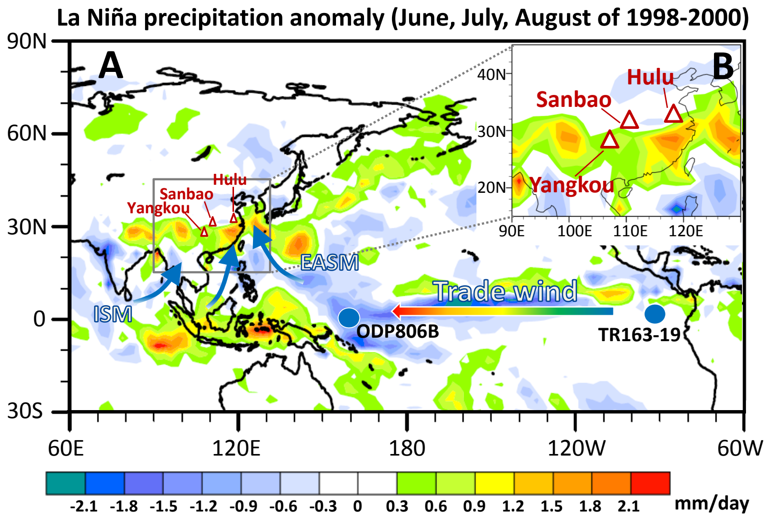

Fig. 1. (A) Map of precipitation anomaly (mm day^{-1}) in June, July, and August (JJA) of 1998–2000 AD during a La Niña event from July 1998 to 2001 April (http://www.cpc.ncep.noaa.gov/products/analysis_monitoring/ensostuff/ensoyears.shtml) comparing with averaged state of JJA from 1980–2010. Triangle symbols denote cave sites of Yangkou (this study), Sanbao (Wang et al., 2008), and Hulu (Cheng et al., 2006). Solid circles indicate marine sediment cores of ODP806B and TR163-19 (Lea et al., 2000). Arrows depict present ground wind directions of the ISM and EASM and also trade wind in the equatorial Pacific. Summer precipitation intensity in eastern and southern China was enhanced during the La Niña event. **(B)** An enlarged map of precipitation anomaly with cave sites of Yangkou, Sanbao, and Hulu.

CPD
9, 6287–6309, 2013

Variability of the Asian summer monsoon

T. -Y. Li et al.

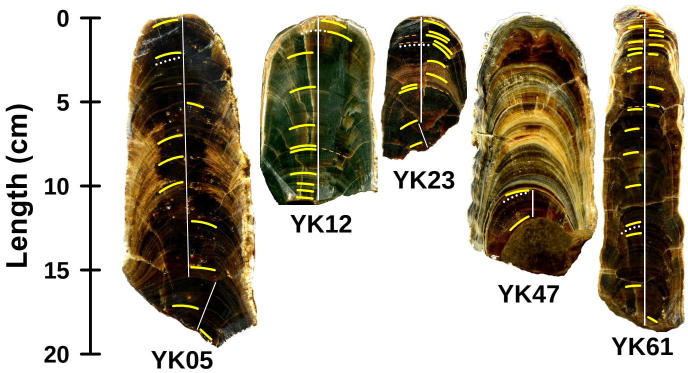

Fig. 2. Photographs of the five stalagmites collected from Yangkou cave. Brown dashed curves show hiatuses. Straight lines represent subsampling routes for oxygen isotope measurement. Yellow curves denote drilled subsamples for ^{230}Th dating. White dots are the subsamples collected for Hendy Test (Hendy, 1971).

CPD
9, 6287–6309, 2013

Variability of the Asian summer monsoon

T. -Y. Li et al.

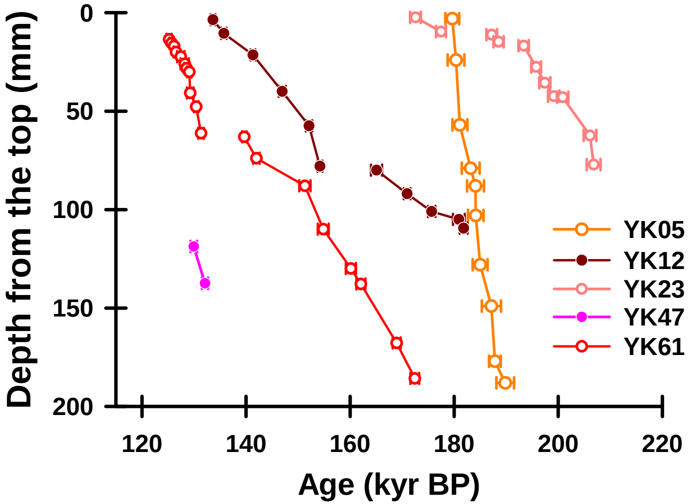

Fig. 3. Age models of Yangkou stalagmites, established with ^{230}Th dates with precisions of ±0.3–1.0 % (horizontal error bars).

CPD
9, 6287–6309, 2013
Variability of the Asian summer monsoon
T. -Y. Li et al.

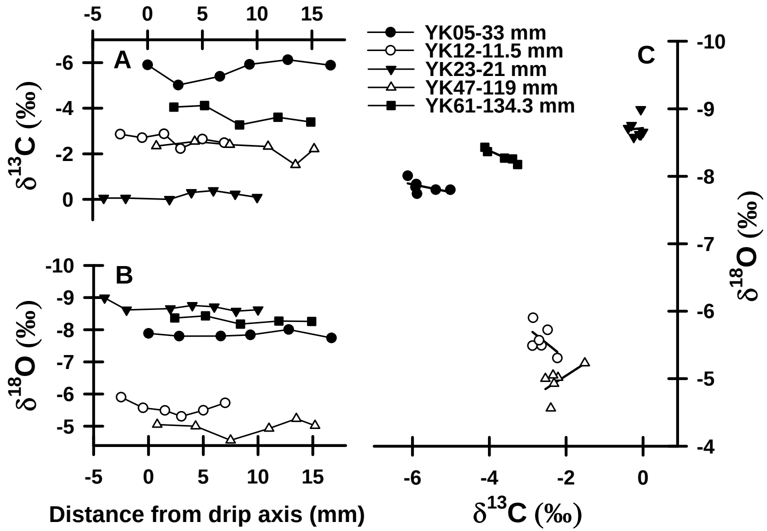

Fig. 4. Hendy Test on the arbitrarily selected laminae of five stalagmites with coeval data of **(A)** δ^{13}C and **(B)** δ^{18}O. **(C)** An absence of relationship between δ^{18}O and δ^{13}C indicates insignificant kinetic fractionation.

CPD
9, 6287–6309, 2013

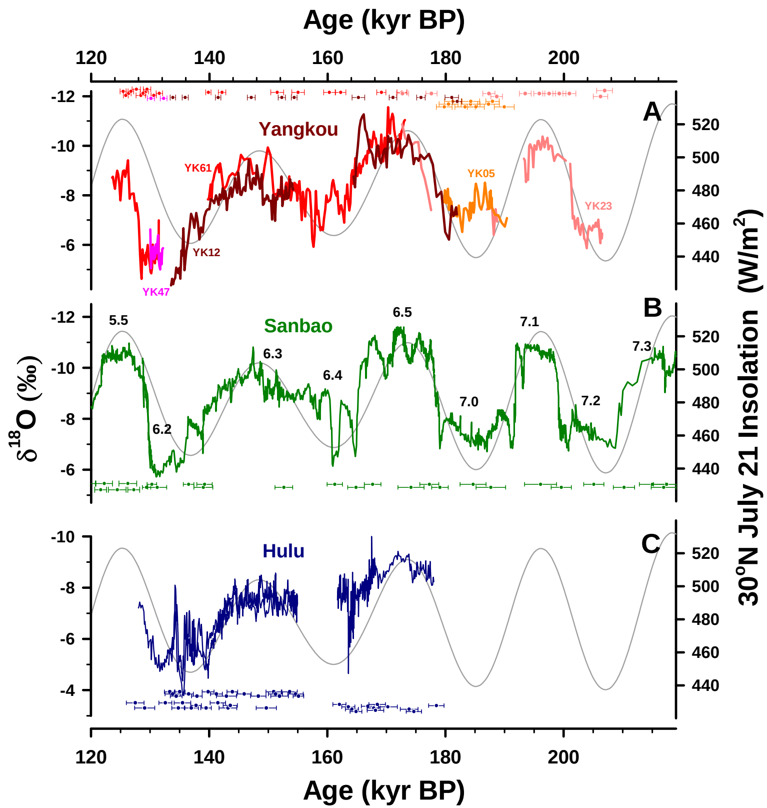

Fig. 5. Cave stalagmite oxygen isotope records of **(A)** Yangkou (this study), **(B)** Sanbao (Wang et al., 2008; Cheng et al., 2009), and **(C)** Hulu (Cheng et al., 2006). ^{230}Th ages and 2-sigma errors were color-coded by stalagmite. Numbers of MIS 5.5–7.3 are given by Sanbao record. Gray line is NHSI on 21 July at 30° N.

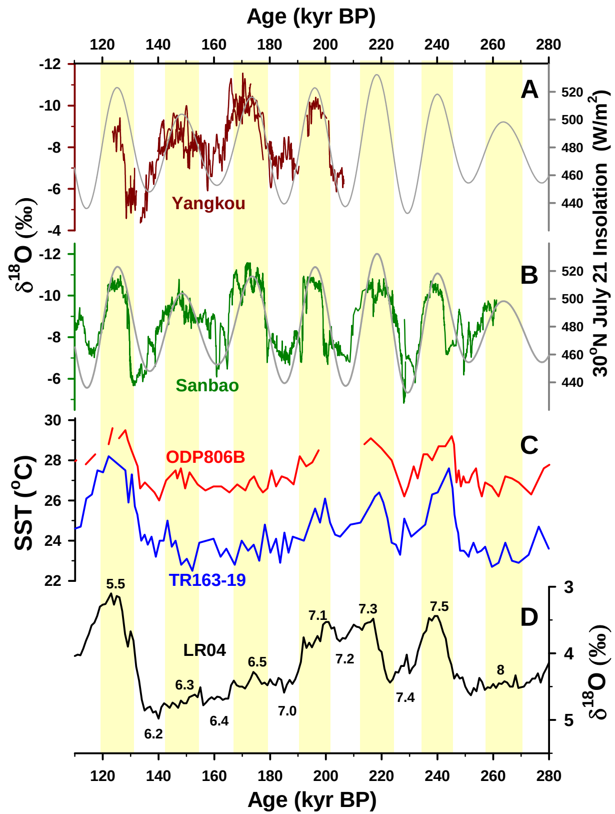

Fig. 6. Comparison of Chinese cave δ^{18}O records of **(A)** Yangkou and **(B)** Sanbao (Wang et al., 2008; Cheng et al., 2009) with **(C)** reconstructed SST records in the WPWP (core ODP806B) and EEP (core TR163-19) (Lea et al., 2000) and **(D)** a global stack benthic foraminifer δ^{18}O sequence LR04 (Lisiecki and Raymo, 2005). Numbers of MIS 5.5–8 are given by LR04 record. Gray line is NHSI on 21 July at 30° N. Vertical bars denote high insolation intervals.

CPD
9, 6287–6309, 2013

Variability of the Asian summer monsoon

T. -Y. Li et al.